RESEARCH PAPER

A model for COVID-19 and bacterial pneumonia coinfection with community- and hospital-acquired infections

Angel G. Cervantes Pérez [iD] [1],*,† and David Adeyemi Oluyori [iD] [2],†

[1]Facultad de Matemáticas, Universidad Autónoma de Yucatán, Mérida, Yucatán, Mexico, [2]Department of Mathematics, School of Physical Science, Ahmadu Bello University, Zaria, Kaduna State, Nigeria

*Corresponding Author
†agcp26@hotmail.com (Angel G. Cervantes Pérez); oluyoridavid@gmail.com (David Adeyemi Oluyori)

Abstract

We propose a new epidemic model to study the coinfection dynamics of COVID-19 and bacterial pneumonia, which is the first model in the literature used to describe mathematically the interaction of these two diseases while considering two infection ways for pneumonia: community-acquired and hospital-acquired transmission. We show that the existence and local stability of equilibria depend on three different parameters, which are interpreted as the basic reproduction numbers of COVID-19, bacterial pneumonia, and bacterial population in the hospital. Numerical simulations are performed to complement our theoretical analysis, and we show that both diseases can persist if the basic reproduction number of COVID-19 is greater than one.

Key words: Coronavirus; bacterial pneumonia; coinfection
AMS 2020 Classification: 34C60; 34D20; 92D30

1 Introduction

The virulent nature of Coronavirus Disease 2019 (COVID-19) has continued to be significant as a public health concern since the WHO declared it a global pandemic in the early part of 2020. Trend analysis has shown that one of the main causes of death resulting from Coronavirus has been attributed to secondary causes due to bacterial and viral infections. As the Coronavirus Disease continues to attract attention from various stakeholders in health and governance, who work relentlessly to unravel its dynamics and curtail its spread through pharmaceutical and non-pharmaceutical methods, studies have shown that Respiratory Tract Infections (RTIs) can predispose patients to coinfections [1, 2]. RTIs are infections of body parts involved in breathing, such as sinuses, throat, airways or lungs, which can be caused by several bacteria and viruses such as influenza [3]. The most significant of these RTIs, which affect the upper respiratory tract include tonsillitis, pharyngitis, sinusitis and certain types of influenza (such as H1N1) [4] with symptoms such as cough, sore throat, nasal congestion, headache, among others.

Historically, according to [5], a large part of the death toll recorded in the 1918 influenza pandemic was due to bacterial infection caused by *Streptococcus pneumoniae*. Evidence from the study in [6] revealed that poor outcomes in the influenza (H1N1) pandemic were associated with coinfections. Aside from H1N1, MERS and SARS-CoV have been identified as major respiratory tract infections in the last decade. These have so far been detected by highly sensitive techniques such as MALDI-TOF and Multiplex PCR. Therefore, the study of coinfections in a pandemic situation such as COVID-19 has become an essential need due to the clinical,

diagnostic and therapeutic challenges it raises [7]. To further buttress the aforestated, Lansbury et al. [8] highlighted some important aspects of bacterial and viral infections in COVID-19 and antimicrobial prescription.

Despite the proven epidemiological significance of coinfections in the severity of respiratory diseases, they are largely understudied during a large outbreak of respiratory infections such as SARS-CoV-2 [9]. According to Zhou et al. [10], it was shown that 50% of the fatalities due to COVID-19 result from secondary bacterial infections. Also, Chen et al. [11] attribute these deaths to bacterial and fungal infections. Furthermore, in [9], clinical evidence has revealed the complexity in the diagnoses of coinfections when the causative virus is resident in the host before the viral infection or has been contacted nosocomially. The authors in [12] reported that patients presenting SARS-CoV-2 infection have a clinical phenotype that is very close to that of bacterial pneumonia.

Mathematical modelling of epidemics has become a crucial tool to forecast the future course of an outbreak, as well as to evaluate possible strategies to control the spread of diseases. The analysis of these models is useful to decide the best course of action to eradicate a disease since it is often less costly to perform numerical simulations than experimental studies. Also, it is easier to determine the different possible outcomes of an epidemic by studying the equilibrium states and the threshold dynamics of a model than to test it in real life. The history of epidemic modelling has developed in relatively recent times. Although an early model was created by Bernoulli in 1760 to evaluate the effectiveness of inoculating healthy people against the smallpox virus [13], deterministic epidemic models became increasingly popular in the early 20th century, starting with Ross's differential equation model on the control of malaria [14]. The susceptible-infectious-recovered model was inspired by the papers by Ross [15] in 1916 and Ross and Hudson [16, 17] in 1917, who studied *a priori* pathometry, followed by Kermack and McKendrick's integro-differential age-structured model [18] in 1927. In subsequent decades, a plethora of epidemic models was studied in the literature, many based on ordinary differential equations (ODEs). Recent works have employed a range of different methods, such as fractional order differential equations, partial differential equations, fuzzy logic, network-based and stochastic models, with the aim to describe the complexities of pathogen transmission. However, the complexity of these methods often precludes an intuitive understanding of the interactions between its variables and parameters [19], and simple models that can be adequately fitted to some epidemic data can be more useful than more complex models that also provide an adequate fit to the same data [20]. Deterministic ODE models have the advantage of having an extensive theory for their theoretical and numerical study [21], they have also been successfully fitted to real-world epidemic data and their prediction accuracy can be improved by methods such as segmentation of epidemic event sequences [22].

During the course of the COVID-19 pandemic, many different works have emerged to model mathematically the spread of SARS-CoV-2. Several recent papers have focused on analyzing the effects of vaccination campaigns [23, 24, 25, 26], as well as the relationship of COVID-19 with conditions such as diabetes [27] and heart attacks [28]. Some authors have incorporated the dynamics of new strains of SARS-CoV-2, such as the Omicron variant [28], while others have developed coinfection models. As a background to our present work, recent studies have established clinical evidence of coinfections of SARS-CoV-2 (COVID-19) with other diseases such as tuberculosis [7, 29, 30, 31, 32, 33], influenza A (H1N1) [34, 35, 36, 37, 38] and Middle East Respiratory Syndrome Coronavirus (MERS-CoV) [39], as well as bacterial coinfections [40]. In response to the foregoing, researchers have developed mathematical models to study the coinfection dynamics of COVID-19. Soni and Singh [41] used a systems biology approach to study a cellular-level model for SARS-CoV-2-influenza coinfection, they performed simulations with the Matlab SimBiology toolbox to suggest therapeutic intervention points. Tchoumi et al. [42] proposed a compartmental population model for coinfection with malaria. They determined conditions for the stability of equilibria, showed that the model may undergo a backward bifurcation and derived conditions for optimal control to mitigate the spread of both diseases. Tuberculosis-COVID-19 coinfection has been modelled by Bandedar and Ghosh [43], who considered a model with waning immunity and performed a bifurcation and stability analysis, as well as simulations using data from India. A different model for tuberculosis coinfection was studied by Rwezaura et al. [44], who investigated the effects of COVID-19 vaccination and treatment control and performed parameter fitting with data from Indonesia. Optimal control for a COVID-19-dengue model was studied by Omame et al. [45] using five controls; furthermore, the authors fitted their model to the cumulative COVID-19 cases and deaths in Brazil. In [46], Omame et al. analyzed a fractional coinfection model for diabetes and COVID-19 using the Atangana-Baleanu derivative. The authors studied the Hyers-Ulams stability and global asymptotic stability and fitted the model to COVID-19 data from Indonesia.

Despite the above-mentioned developments in the literature, no model has been proposed to study the coinfection dynamics of COVID-19 with bacterial pneumonia. Bacterial pneumonia is an inflammation of the lungs caused by infection with certain bacteria. Depending on the location where a person acquires the infection, it can be classified as either *community-acquired pneumonia* or *hospital-acquired pneumonia*. Community-acquired pneumonia is by far the most common type [47]. On the other hand, hospital-acquired pneumonia is usually more severe because the infecting organisms tend to be more aggressive, less likely to respond to antibiotics and harder to treat [48]. In this vein, we see from [49, 50, 51] that clinical studies have shown that critically ill COVID-19 patients admitted to the hospital suffer more frequent bacterial or fungal nosocomial infections, and patients with underlying risk factors such as advanced age, mechanical ventilation or prolonged hospital stay are more prone to these complications. Moreover, patients with mild COVID-19 infection are less likely to develop a more severe disease as a result of confection upon admission to medical facilities compared to those with high-risk factors due to bacterial and fungal infections.

In view of the above evidence, we think that there is a need to mathematically study the coinfection dynamics of COVID-19 with bacterial pneumonia. However, none of the models mentioned above has the structure necessary to be applied to this disease, considering that bacterial infections can be acquired both in the community and in the hospital. Hence, we aim to study here a new ODE model tailored specially to these needs. In contrast to the work by Giannella et al. [40], who developed a predictive model to stratify the risk of bacterial coinfection based on an observational study of hospitalised COVID-19 patients, we intend to use a theoretical approach of compartmental ODE models, which allows us to make simulations not only for the hospitalised subpopulation but in the community at large.

This paper is structured as follows: in Section 2, we introduce three models: a sub-model for COVID-19 infection, a sub-model for bacterial pneumonia, and a coinfection model that includes the dynamics of both diseases. In Section 3, we determine some basic properties for the two sub-models. In Section 4, we provide an analysis of the coinfection model. In Section 5, we perform some numerical simulations to illustrate the dynamics of the coinfection model. Finally, we provide a summary and discussion of our results in Section 6 and some concluding remarks in Section 7.

2 Description of the models

COVID-19 infection model

The COVID-19 infection model subdivides the human population into four compartments: susceptible (S), infected but not hospitalised (I), hospitalised (H), and recovered (R). This model can be described by the following system of equations:

$$
\begin{aligned}
S' &= \Lambda + \sigma R - \mu S - \alpha S I, \\
I' &= \alpha S I - (\gamma + \eta + \mu) I, \\
H' &= \eta I - (\theta + \delta + \mu) H, \\
R' &= \gamma I + \theta H - \mu R - \sigma R.
\end{aligned}
\tag{1}
$$

The interpretation of parameters is as follows:

- Λ: recruitment rate of susceptible population.
- μ: natural death rate.
- α: transmission rate of COVID-19.
- γ: recovery rate of people infected with COVID-19 but not hospitalised.
- θ: recovery rate of hospitalised people.
- η: hospitalisation rate.
- δ: COVID-19-induced death rate of hospitalised people.
- σ: rate of loss of immunity against COVID-19 infection.

For model (1), we assume that COVID-19 is transmitted by contact between susceptible and infected (but not hospitalised) people at a bilinear rate $\alpha S I$. A portion of the infected population is admitted to hospitals at a rate η. The average recovery time is $1/\gamma$ for non-hospitalised people and $1/\theta$ for hospitalised people. Further, we assume that only hospitalised patients may have a COVID-19-induced death. Lastly, people recovered from infection lose their natural immunity after an average time $1/\sigma$.

Bacterial pneumonia infection model

The model for bacterial pneumonia subdivides the human population into three compartments: susceptible (S), infected (I), and recovered (R). We also consider a compartment B representing the population of bacteria in the environment. The model is given by the following system:

$$
\begin{aligned}
S' &= \Lambda - \mu S - b S I - b_1 S B, \\
I' &= b S I + b_1 S B - \phi I - \mu I - \delta I, \\
R' &= \phi I - \mu R, \\
B' &= p I + r B \left(1 - \frac{B}{\kappa} \right) - m B.
\end{aligned}
\tag{2}
$$

The parameters of this model can be interpreted as follows:

- Λ: recruitment rate of susceptible population.
- μ: natural death rate.
- b: transmission rate of community-acquired bacterial pneumonia.
- b_1: transmission rate of hospital-acquired bacterial pneumonia.
- δ: disease-induced death rate of infected population.
- ϕ: recovery rate of people with bacterial infection.
- p: rate of excretion of bacteria in the environment by infected people.
- r: maximal per capita growth rate of bacteria in the environment.
- κ: carrying capacity of bacterial population.
- m: clearance rate of bacterial population.

For model (2), we assume that susceptible people get community-acquired pneumonia at a rate $b S I$ and hospital-acquired pneumonia at a rate $b_1 S B$. Infected people have a pneumonia-induced death rate δ and may recover at a rate ϕ. The population of bacteria in the environment follows a logistic growth rate and may additionally increase at a rate proportional to the number of infected people.

Coinfection model

Based on models (1) and (2), we propose a combined COVID-19–bacterial pneumonia coinfection model. We will consider three stages for COVID-19 infection and four for bacterial infection, which gives twelve mutually exclusive compartments: bacterial pneumonia susceptible and COVID-19 susceptible (X_{SS}); bacterial pneumonia susceptible and COVID-19 mildly infected (X_{SI}); bacterial pneumonia susceptible and COVID-19 hospitalised (X_{SH}); bacterial pneumonia susceptible and COVID-19 recovered (X_{SR}); bacterial pneumonia infected and COVID-19 susceptible (X_{IS}); bacterial pneumonia infected and COVID-19 mildly infected (X_{II}); bacterial pneumonia infected and COVID-19 hospitalised (X_{IH}); bacterial pneumonia infected and COVID-19 recovered (X_{IR}); bacterial pneumonia recovered and COVID-19 susceptible (X_{RS}); bacterial pneumonia recovered and COVID-19 mildly infected (X_{RI}); bacterial pneumonia recovered and COVID-19 hospitalised (X_{RH}); and bacterial pneumonia recovered and COVID-19 recovered (X_{RR}). Additionally, we consider a compartment B representing concentration of bacteria in the hospital environment. We make the following assumptions:

  i. COVID-19 is transmitted by contact with people in the X_{SI}, X_{II} and X_{RI} compartments.
  ii. The population susceptible to COVID-19 are infected by this disease at a rate α_1 if they have bacterial pneumonia, and at a rate α otherwise.
  iii. The hospitalisation rate for people coinfected with COVID-19 and community-acquired pneumonia increases by an amount η_1 with respect to people with only COVID-19.
  iv. The COVID-19 recovery rate for hospitalised people is θ_1 if they are coinfected, and θ otherwise.
  v. Non-hospitalised people get community-acquired pneumonia by contact with people in the X_{IS}, X_{II} and X_{IR} compartments.
  vi. Non-hospitalised people are infected with pneumonia at a rate b_1 if they have COVID-19, and at a rate b otherwise.
  vii. People hospitalised due to COVID-19 get hospital-acquired pneumonia at a rate proportional to the concentration of bacteria in the environment.
  viii. The disease-induced death rate for coinfected hospitalised patients is increased by an amount δ_2 with respect to those with only COVID-19.
  ix. The pneumonia-induced death rate for non-hospitalised people is δ_0 if they have COVID-19, and δ otherwise.
  x. The pneumonia recovery rate is ϕ_1 for people in the X_{II} compartment, ϕ_2 for the X_{IH} compartment, and ϕ for the X_{IS} and X_{IR} compartments.

The schematic diagram of model (3) can be seen in Figure 1. All parameters are assumed to be positive.
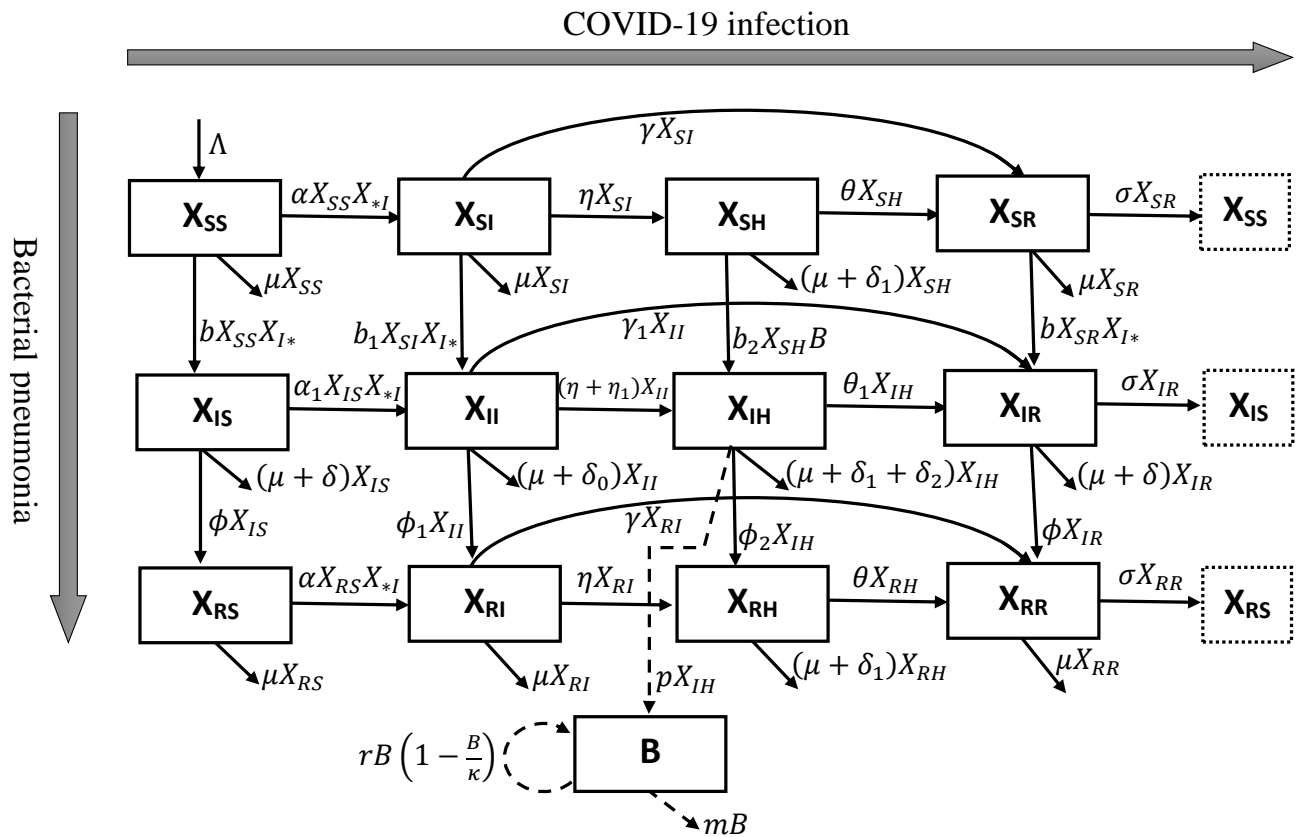
Figure 1. Schematic diagram of the coinfection model. Solid lines represent the transition between compartments. Dashed lines represent the proliferation of bacteria. X_{*I} denotes $X_{SI} + X_{II} + X_{RI}$ and X_{I*} denotes $X_{IS} + X_{II} + X_{IR}$.

The above assumptions yield a coinfection model given by the following system of 13 differential equations:

$$
\begin{aligned}
X'_{SS} &= \Lambda + \sigma X_{SR} - \mu X_{SS} - \alpha X_{SS}(X_{SI} + X_{II} + X_{RI}) - b X_{SS}(X_{IS} + X_{II} + X_{IR}), \\
X'_{SI} &= \alpha X_{SS}(X_{SI} + X_{II} + X_{RI}) - (\gamma + \eta + \mu)X_{SI} - b_1 X_{SI}(X_{IS} + X_{II} + X_{IR}), \\
X'_{SH} &= \eta X_{SI} - \theta X_{SH} - (\mu + \delta_1)X_{SH} - b_2 X_{SH}B, \\
X'_{SR} &= \gamma X_{SI} + \theta X_{SH} - \mu X_{SR} - \sigma X_{SR} - b X_{SR}(X_{IS} + X_{II} + X_{IR}), \\
X'_{IS} &= \sigma X_{IR} + b X_{SS}(X_{IS} + X_{II} + X_{IR}) - \alpha_1 X_{IS}(X_{SI} + X_{II} + X_{RI}) - (\mu + \delta)X_{IS} - \phi X_{IS}, \\
X'_{II} &= b_1 X_{SI}(X_{IS} + X_{II} + X_{IR}) + \alpha_1 X_{IS}(X_{SI} + X_{II} + X_{RI}) - (\gamma_1 + \eta + \eta_1 + \mu + \delta_0 + \phi_1)X_{II}, \\
X'_{IH} &= (\eta + \eta_1)X_{II} + b_2 X_{SH}B - \theta_1 X_{IH} - (\mu + \delta_1 + \delta_2)X_{IH} - \phi_2 X_{IH}, \\
X'_{IR} &= b X_{SR}(X_{IS} + X_{II} + X_{IR}) + \gamma_1 X_{II} + \theta_1 X_{IH} - (\mu + \delta)X_{IR} - \phi X_{IR} - \sigma X_{IR}, \\
X'_{RS} &= \sigma X_{RR} + \phi X_{IS} - \mu X_{RS} - \alpha X_{RS}(X_{SI} + X_{II} + X_{RI}), \\
X'_{RI} &= \phi_1 X_{II} + \alpha X_{RS}(X_{SI} + X_{II} + X_{RI}) - (\gamma + \eta + \mu)X_{RI}, \\
X'_{RH} &= \eta X_{RI} + \phi_2 X_{IH} - \theta X_{RH} - (\mu + \delta_1)X_{RH}, \\
X'_{RR} &= \phi X_{IR} + \gamma X_{RI} + \theta X_{RH} - \mu X_{RR} - \sigma X_{RR}, \\
B' &= p X_{IH} + rB\left(1 - \frac{B}{\kappa}\right) - mB.
\end{aligned}
\tag{3}
$$

3 Analysis of sub-models

Before studying the dynamics of the coinfection model (3), we will analyze the two sub-models (COVID-19 only and bacterial pneumonia only).

Analysis of the COVID-19 infection model

The COVID-19-only model (1) has a disease-free equilibrium (DFE) given by

$$
\mathcal{E}_{C0} = (S, I, H, R) = \left(\frac{\Lambda}{\mu}, 0, 0, 0\right).
$$

The stability of $\mathcal{E}_{C0}$ depends on the basic reproduction number of model (1).

Theorem 1 *Let*

$$
\mathcal{R}_C = \frac{\alpha \Lambda}{\mu(\gamma + \eta + \mu)}.
\tag{4}
$$

Then, the disease-free equilibrium $\mathcal{E}_{C0}$ of model (1) is locally asymptotically stable if $\mathcal{R}_C < 1$, but unstable if $\mathcal{R}_C > 1$.

Proof 1 *Using the notation in [52], we define the matrix of new infections $\mathcal{F}$ and the transition matrix $\mathcal{V} = \mathcal{V}^- - \mathcal{V}^+$ by*

$$
\mathcal{F} = \begin{bmatrix} \alpha S I \\ 0 \end{bmatrix}, \qquad
\mathcal{V}^- = \begin{bmatrix} (\gamma + \eta + \mu)I \\ (\theta + \delta + \mu)H \end{bmatrix}, \qquad
\mathcal{V}^+ = \begin{bmatrix} 0 \\ \eta I \end{bmatrix}.
$$

Then, we compute the matrices $F = D\mathcal{F}(\mathcal{E}_{C0})$ and $V = D\mathcal{V}(\mathcal{E}_{C0})$, as follows:

$$
F = \begin{bmatrix} \frac{\alpha \Lambda}{\mu} & 0 \\ 0 & 0 \end{bmatrix}, \qquad
V = \begin{bmatrix} \gamma + \eta + \mu & 0 \\ -\eta & \theta + \delta + \mu \end{bmatrix}.
$$

The basic reproduction number $\mathcal{R}_C$ of the COVID-19-only model is given by the spectral radius of FV^{-1}. From this, we obtain that $\mathcal{R}_C$ is given by (4).
By an application of [52, Theorem 2], we conclude that $\mathcal{E}_{C0}$ is locally asymptotically stable if $\mathcal{R}_C < 1$ and unstable if $\mathcal{R}_C > 1$.

Analysis of the bacterial pneumonia infection model

The bacterial pneumonia model (2) has a DFE given by

$$
\mathcal{E}_{P0} = (S, I, R, B) = \left(\frac{\Lambda}{\mu}, 0, 0, 0\right).
$$

The stability of $\mathcal{E}_{P0}$ will depend on a parameter $\mathcal{R}_P$, as detailed in the following result.

Theorem 2 *Let*

$$
\mathcal{R}_P = \frac{b\Lambda}{\mu(\phi + \mu + \delta)}.
\tag{5}
$$

Then, the disease-free equilibrium $\mathcal{E}_{P_0}$ of model (2) is locally asymptotically stable if $\mathcal{R}_P < 1$, but unstable if $\mathcal{R}_P > 1$.

Proof 2 *Using the notation in [52], we define the matrix of new infections $\mathcal{F}$ and the transition matrix $\mathcal{V} = \mathcal{V}^- - \mathcal{V}^+$ by*

$$\mathcal{F} = \begin{bmatrix} bSI + b_1 SB \end{bmatrix}, \qquad \mathcal{V}^- = \begin{bmatrix} (\phi + \mu + \delta)I \end{bmatrix}, \qquad \mathcal{V}^+ = \begin{bmatrix} 0 \end{bmatrix}.$$

To apply the next-generation matrix method, we compute $F = D\mathcal{F}(\mathcal{E}_{C_0})$ and $V = D\mathcal{V}(\mathcal{E}_{C_0})$, which are given by

$$F = \begin{bmatrix} \frac{b\Lambda}{\mu} \end{bmatrix}, \qquad V = \begin{bmatrix} \phi + \mu + \delta \end{bmatrix}.$$

Using the same method as before, we obtain the basic reproduction number $\mathcal{R}_P$ of the bacterial pneumonia-only model as the spectral radius of FV^{-1}, which gives the expression (5).

Finally, by [52, Theorem 2], we conclude that $\mathcal{E}_{P_0}$ is locally asymptotically stable if $\mathcal{R}_P < 1$ and unstable if $\mathcal{R}_P > 1$.

4   Analysis of the COVID-19–bacterial pneumonia coinfection model

Next, we consider the dynamics of the coinfection model (3). The existence and stability of equilibria for model (3) will depend on three parameters, which are defined as follows:

$$\mathcal{R}_C := \frac{\alpha\Lambda}{\mu(\gamma + \eta + \mu)}, \qquad \mathcal{R}_P := \frac{b\Lambda}{\mu(\phi + \mu + \delta)}, \qquad \mathcal{R}_B := \frac{r}{m}.$$

As we saw in the previous section, the parameters $\mathcal{R}_C$ and $\mathcal{R}_P$ represent the basic reproduction numbers of COVID-19 and bacterial pneumonia, respectively. On the other hand, $\mathcal{R}_B$ can be interpreted as the reproduction number of bacterial population in the hospital.

Equilibria of the model

By direct computation, we obtain the following result about the equilibria of model (3).

Theorem 3 *The coinfection model (3) has the following steady states:*

   i. *The disease-free, bacterial population-free equilibrium:*

$$\mathcal{E}_0 = \left(X_{SS}^{(0)}, 0, 0, 0, 0, 0, 0, 0, 0, 0, 0, 0 \right),$$

   where

$$X_{SS}^{(0)} = \frac{\Lambda}{\mu}.$$

   ii. *The disease-free, bacterial population-present equilibrium:*

$$\mathcal{E}_1 = \left(X_{SS}^{(1)}, 0, 0, 0, 0, 0, 0, 0, 0, 0, 0, B^{(1)} \right),$$

   where

$$X_{SS}^{(1)} = \frac{\Lambda}{\mu}, \qquad B^{(1)} = \frac{\kappa}{r}(r - m).$$

   This equilibrium exists if and only if $\mathcal{R}_B > 1$.
   iii. *The COVID-19-free, pneumonia-present, bacterial population-free equilibrium:*

$$\mathcal{E}_2 = \left(X_{SS}^{(2)}, 0, 0, 0, X_{IS}^{(2)}, 0, 0, 0, X_{RS}^{(2)}, 0, 0, 0, 0 \right),$$

   where

$$X_{SS}^{(2)} = \frac{\mu + \delta + \phi}{b}, \qquad X_{IS}^{(2)} = \frac{\Lambda}{\mu + \delta + \phi} - \frac{\mu}{b}, \qquad X_{RS}^{(2)} = \frac{\phi}{\mu} X_{IS}^{(2)}.$$

   This equilibrium exists if and only if $\mathcal{R}_P > 1$.
   iv. *The COVID-19-free, pneumonia-present, bacterial population-present equilibrium:*

$$\mathcal{E}_3 = \left(X_{SS}^{(3)}, 0, 0, 0, X_{IS}^{(3)}, 0, 0, 0, X_{RS}^{(3)}, 0, 0, 0, B^{(3)} \right),$$

where

$$X_{SS}^{(3)} = \frac{\mu + \delta + \phi}{b}, \qquad X_{IS}^{(3)} = \frac{\Lambda}{\mu + \delta + \phi} - \frac{\mu}{b}, \qquad X_{RS}^{(3)} = \frac{\phi}{\mu} X_{IS}^{(3)},$$

$$B^{(3)} = \frac{\kappa}{r}(r - m).$$

This equilibrium exists if and only if

$$\mathcal{R}_B > 1 \quad and \quad \mathcal{R}_P > 1.$$

v. The COVID-19-present, pneumonia-free, bacterial population-free equilibrium:

$$\mathcal{E}_4 = \left(X_{SS}^{(4)}, X_{SI}^{(4)}, X_{SH}^{(4)}, X_{SR}^{(4)}, 0, 0, 0, 0, 0, 0, 0, 0, 0 \right),$$

where

$$X_{SS}^{(4)} = \frac{\gamma + \eta + \mu}{\alpha}, \qquad X_{SI}^{(4)} = \frac{(\mu + \sigma)(\theta + \mu + \delta_1)\left[\alpha\Lambda - \mu(\gamma + \eta + \mu)\right]}{\alpha\left[\mu(\theta + \mu + \delta_1)(\gamma + \eta + \mu + \sigma) + \eta\sigma(\mu + \delta_1)\right]},$$

$$X_{SH}^{(4)} = \frac{\eta}{\theta + \mu + \delta_1} X_{SI}^{(4)}, \qquad X_{SR}^{(4)} = \left(\frac{\gamma}{\mu + \sigma} + \frac{\eta\theta}{(\mu + \sigma)(\theta + \mu + \delta_1)} \right) X_{SI}^{(4)}.$$

This equilibrium exists if and only if

$$\mathcal{R}_C > 1.$$

Proof 3 *Equilibria $\mathcal{E}_0$, $\mathcal{E}_1$, $\mathcal{E}_2$ and $\mathcal{E}_3$ are obtained by assuming that $X_{SI} = 0$ in the system at equilibrium and solving the resulting algebraic equations. This yields four different cases: one for each equilibrium.*
On the other hand, assuming $X_{SI} > 0$ and $X_{IS} = 0$ results in only one case, corresponding to the equilibrium $\mathcal{E}_4$.
The case when $X_{SI} > 0$ and $X_{IS} > 0$ will be discussed below.

Theorem 3 shows that, under certain conditions, the coinfection model has five different steady states. Moreover, we conjecture that a sixth equilibrium, with positive values for all variables, may exist. We will denote this interior equilibrium by $\mathcal{E}_5$. Since the theoretical analysis becomes too cumbersome in this case, we will resort to numerical simulations to investigate the dynamics of equilibrium $\mathcal{E}_5$ (see Section 5).

Stability analysis

We will now analyze the local stability for the equilibria of system (3) by means of the linearisation method and the Hartman–Grobman theorem. Our results will focus only on the disease-free equilibria $\mathcal{E}_0$ and $\mathcal{E}_1$.

Theorem 4

(i) *The disease-free, bacterial population-free equilibrium $\mathcal{E}_0$ is locally asymptotically stable if*

$$\mathcal{R}_C < 1, \quad \mathcal{R}_P < 1 \quad and \quad \mathcal{R}_B < 1, \tag{6}$$

and it is unstable if one of $\mathcal{R}_C > 1$, $\mathcal{R}_P > 1$ or $\mathcal{R}_B > 1$ holds.
(ii) *The disease-free, bacterial population-present equilibrium $\mathcal{E}_1$ is locally asymptotically stable if*

$$\mathcal{R}_C < 1, \quad \mathcal{R}_P < 1 \quad and \quad \mathcal{R}_B > 1, \tag{7}$$

and it is unstable if one of $\mathcal{R}_C > 1$, $\mathcal{R}_P > 1$ or $\mathcal{R}_B < 1$ holds.

Proof 4 *The Jacobian of system (3) evaluated at $\mathcal{E}_0$ is given by*

$$J_0 = \begin{bmatrix}
-\mu & -\frac{\alpha\Lambda}{\mu} & 0 & \sigma & -\frac{b\Lambda}{\mu} & -\frac{(\alpha+b)\Lambda}{\mu} & 0 & -\frac{b\Lambda}{\mu} & 0 & -\frac{\alpha\Lambda}{\mu} & 0 & 0 & 0 \\
0 & \frac{\alpha\Lambda}{\mu} - k_1 & 0 & 0 & 0 & \frac{\alpha\Lambda}{\mu} & 0 & 0 & 0 & \frac{\alpha\Lambda}{\mu} & 0 & 0 & 0 \\
0 & \eta & -k_2 & 0 & 0 & 0 & 0 & 0 & 0 & 0 & 0 & 0 & 0 \\
0 & \gamma & \theta & -k_3 & 0 & 0 & 0 & 0 & 0 & 0 & 0 & 0 & 0 \\
0 & 0 & 0 & 0 & \frac{b\Lambda}{\mu} - k_4 & \frac{b\Lambda}{\mu} & 0 & \frac{b\Lambda}{\mu} + \sigma & 0 & 0 & 0 & 0 & 0 \\
0 & 0 & 0 & 0 & 0 & -k_5 & 0 & 0 & 0 & 0 & 0 & 0 & 0 \\
0 & 0 & 0 & 0 & 0 & \eta + \eta_1 & -\theta_1 - k_6 & 0 & 0 & 0 & 0 & 0 & 0 \\
0 & 0 & 0 & 0 & 0 & \gamma_1 & \theta_1 & -k_7 & 0 & 0 & 0 & 0 & 0 \\
0 & 0 & 0 & 0 & \phi & 0 & 0 & 0 & -\mu & 0 & 0 & \sigma & 0 \\
0 & 0 & 0 & 0 & 0 & \phi_1 & 0 & 0 & 0 & -k_1 & 0 & 0 & 0 \\
0 & 0 & 0 & 0 & 0 & 0 & \phi_2 & 0 & 0 & \eta & -k_2 & 0 & 0 \\
0 & 0 & 0 & 0 & 0 & 0 & 0 & \phi & 0 & \gamma & \theta & -k_3 & 0 \\
0 & 0 & 0 & 0 & 0 & 0 & p & 0 & 0 & 0 & 0 & 0 & r - m
\end{bmatrix},$$

where

$$k_1 = \gamma + \eta + \mu, \qquad k_2 = \theta + \mu + \delta_1, \qquad k_3 = \mu + \sigma, \qquad k_4 = \mu + \delta + \phi,$$

$$k_5 = \gamma_1 + \eta + \eta_1 + \mu + \delta_0 + \phi_1, \qquad k_6 = \mu + \delta_1 + \delta_2 + \phi_2, \qquad k_7 = \mu + \delta + \phi + \sigma.$$

From this, we obtain the characteristic polynomial

$$(\lambda + \mu)^2 (\lambda + k_1)(\lambda + k_2)^2 (\lambda + k_3)^2 (\lambda + k_5)(\lambda + \theta_1 + k_6)(\lambda + k_7)$$

$$\times \left(\lambda + k_1 - \frac{\alpha\Lambda}{\mu}\right)\left(\lambda + k_4 - \frac{b\Lambda}{\mu}\right)(\lambda + m - r) = 0.$$

By the Hartman−Grobman theorem [53, p. 311], we know that the solutions of (3) and its linearisation are qualitatively equivalent near $\mathcal{E}_0$ provided that $\mathcal{E}_0$ is a hyperbolic equilibrium. Due to positivity of parameters, it is clear that all eigenvalues have negative real part if and only if

$$\gamma + \eta + \mu - \frac{\alpha\Lambda}{\mu} > 0, \qquad \mu + \delta + \phi - \frac{b\Lambda}{\mu} > 0 \qquad and \qquad m - r > 0,$$

which is equivalent to the condition (6). On the other hand, the opposite inequalities guarantee that there is at least one eigenvalue with positive real part and no eigenvalues with zero real part. Hence, we can conclude part (i) of the theorem.

Next, we compute the Jacobian at $\mathcal{E}_1$, which is given by

$$J_1 = \begin{bmatrix}
-\mu & -\frac{\alpha\Lambda}{\mu} & 0 & \sigma & -\frac{b\Lambda}{\mu} & -\frac{(\alpha+b)\Lambda}{\mu} & 0 & -\frac{b\Lambda}{\mu} & 0 & -\frac{\alpha\Lambda}{\mu} & 0 & 0 & 0 \\
0 & \frac{\alpha\Lambda}{\mu} - k_1 & 0 & 0 & 0 & \frac{\alpha\Lambda}{\mu} & 0 & 0 & 0 & \frac{\alpha\Lambda}{\mu} & 0 & 0 & 0 \\
0 & \eta & -k_0 - k_2 & 0 & 0 & 0 & 0 & 0 & 0 & 0 & 0 & 0 & 0 \\
0 & \gamma & \theta & -k_3 & 0 & 0 & 0 & 0 & 0 & 0 & 0 & 0 & 0 \\
0 & 0 & 0 & 0 & \frac{b\Lambda}{\mu} - k_4 & \frac{b\Lambda}{\mu} & 0 & \frac{b\Lambda}{\mu} + \sigma & 0 & 0 & 0 & 0 & 0 \\
0 & 0 & 0 & 0 & 0 & -k_5 & 0 & 0 & 0 & 0 & 0 & 0 & 0 \\
0 & 0 & k_0 & 0 & 0 & \eta + \eta_1 & -\theta_1 - k_6 & 0 & 0 & 0 & 0 & 0 & 0 \\
0 & 0 & 0 & 0 & 0 & \gamma_1 & \theta_1 & -k_7 & 0 & 0 & 0 & 0 & 0 \\
0 & 0 & 0 & 0 & \phi & 0 & 0 & 0 & -\mu & 0 & 0 & \sigma & 0 \\
0 & 0 & 0 & 0 & 0 & \phi_1 & 0 & 0 & 0 & -k_1 & 0 & 0 & 0 \\
0 & 0 & 0 & 0 & 0 & 0 & \phi_2 & 0 & 0 & \eta & -k_2 & 0 & 0 \\
0 & 0 & 0 & 0 & 0 & 0 & 0 & \phi & 0 & \gamma & \theta & -k_3 & 0 \\
0 & 0 & 0 & 0 & 0 & 0 & p & 0 & 0 & 0 & 0 & 0 & m - r
\end{bmatrix},$$

where $k_0 = b_2\kappa\left(1 - \frac{m}{r}\right)$, and $k_1, \ldots, k_7$ are as defined above. Notice that $k_0 > 0$ if and only if $\mathcal{R}_B > 1$.

The characteristic polynomial at $\mathcal{E}_1$ is

$$(\lambda + \mu)^2 (\lambda + k_1)(\lambda + k_2)(\lambda + k_3)^2 (\lambda + k_5)(\lambda + \theta_1 + k_6)(\lambda + k_7)$$

$$\times (\lambda + k_0 + k_2)\left(\lambda + k_1 - \frac{\alpha\Lambda}{\mu}\right)\left(\lambda + k_4 - \frac{b\Lambda}{\mu}\right)(\lambda + r - m) = 0.$$

It follows that all eigenvalues have negative real part if and only if

$$k_0 + k_2 > 0, \quad \gamma + \eta + \mu - \frac{\alpha\Lambda}{\mu} > 0, \quad \mu + \delta + \phi - \frac{b\Lambda}{\mu} > 0 \quad and \quad r - m > 0.$$

The first of these inequalities holds automatically when $\mathcal{R}_B > 1$. Hence, we can see that all eigenvalues have negative real part if and only if the last three inequalities hold, and this is equivalent to condition (7). Otherwise, if $\mathcal{R}_C > 1$, $\mathcal{R}_P > 1$ or $\mathcal{R}_B < 1$, there will be at least one eigenvalue with positive real part and no eigenvalues with zero real part. Applying the Hartman−Grobman theorem as before, the proof of (ii) is complete.

5 Numerical analysis

In this section, we perform some simulations for system (3) to illustrate the dynamics of the coinfection model in some cases that are not covered by the analysis in Section 4. We will consider the initial conditions

$$X_{SS}(0) = 8.33 \times 10^7, \quad X_{SI}(0) = 10^5, \quad X_{SH}(0) = 10^3, \quad X_{SR}(0) = 10^5, \quad X_{IS}(0) = 10^3,$$

$$B(0) = 0.8, \quad X_{II}(0) = X_{IH}(0) = X_{IR}(0) = X_{RS}(0) = X_{RI}(0) = X_{RH}(0) = X_{RR}(0) = 0,$$

which represent a case when a fraction of the population is infected with either COVID-19 or bacterial pneumonia, but there are initially no people coinfected with both diseases.

Throughout this section, we will use the parameter values shown in Table 1. The parameters related to demography (Λ and μ) and COVID-19 dynamics (σ, α and α_1) are based on the values used in [54]. Since the literature regarding the modelling of bacterial pneumonia dynamics is scarce, the rest of the parameter values are not based on specific models or real data sets. Instead, we use generic values to show the different dynamics of our model.

Thus, we obtain a fixed value for $\mathcal{R}_C$, which is greater than one ($\mathcal{R}_C = 1.2294$), while $\mathcal{R}_P$ and $\mathcal{R}_B$ will vary as the parameters b and r take different values.

Table 1. Parameter values used for the coinfection model.

Parameter	Value	Unit
Λ	2000	people/day
μ	2.4×10^{-5}	$(\text{people} \cdot \text{day})^{-1}$
σ	1/100	day^{-1}
γ	1/12	day^{-1}
γ_1	1/20	day^{-1}
θ	1/14	day^{-1}
θ_1	1/24	day^{-1}
b_1	2×10^{-9}	$(\text{people} \cdot \text{day})^{-1}$
b_2	0.1	day^{-1}
δ	0.001	day^{-1}
δ_0	0.005	day^{-1}
δ_1	0.01	day^{-1}
δ_2	0.2	day^{-1}
η	0.12	day^{-1}
η_1	0.1	day^{-1}
ϕ	1/14	day^{-1}
ϕ_1	1/30	day^{-1}
ϕ_2	1/40	day^{-1}
p	10^{-5}	$(\text{people} \cdot \text{day})^{-1}$
κ	1	
m	0.01	day^{-1}
α	3×10^{-9}	$(\text{people} \cdot \text{day})^{-1}$
α_1	10^{-8}	$(\text{people} \cdot \text{day})^{-1}$
b	variable	$(\text{people} \cdot \text{day})^{-1}$
r	variable	day^{-1}

Case 1. When $b = 10^{-10}$ and $r = 0.004$, we have $\mathcal{R}_P = 0.1150 < 1$ and $\mathcal{R}_B = 0.4 < 1$. The time plots of the solutions for this case are shown in Figure 2. The solutions converge to a positive equilibrium

$$\mathcal{E}_5 \approx (6.3418 \times 10^7, \ 5684, \ 3153, \ 69716, \ 191.8, \ 0.0735, \ 1537, \ 776.8, 4.368 \times 10^6, \ 391.5, \ 1048, \ 16263, \ 1.3487).$$

As we can see in Figure 2, the population infected with pneumonia presents a peak during the first 200 days, after which it oscillates until settling down to the equilibrium value. The majority of the coinfected population consists of hospitalised individuals (X_{IH}), which reach a peak of 760 000, while the coinfected non-hospitalised population (X_{II}) grows to less than 10 000 individuals. For people recovered from bacterial pneumonia, a similar relationship is seen: there are more hospitalised than non-hospitalised individuals; however, for individuals susceptible to pneumonia, the opposite occurs.

Case 2. When $b = 9 \times 10^{-10}$ and $r = 0.004$, we have $\mathcal{R}_P = 1.0352 > 1$ and $\mathcal{R}_B = 0.4 < 1$. The time plots of the solutions are depicted in Figure 3; we can see that they converge to a positive equilibrium

$$\mathcal{E}_5 \approx (5.711 \times 10^7, \ 5602, \ 3130, \ 6.89 \times 10^4, \ 2229, \ 0.59, \ 1509, \ 765, 1.066 \times 10^7, \ 1046, \ 2005, \ 2.85 \times 10^4, \ 1.33).$$

As seen in Figure 3, the dynamics, in this case, are mostly similar to those of Case 1. The largest difference is the increase in the population infected with pneumonia only (X_{IS}), which reaches a peak about 10 times larger than in Case 1. Also notable is the increase in the population recovered from pneumonia and infected by COVID–19 (X_{RI}), whose peak and equilibrium values are about 3 times larger than in Case 1.

Case 3. When $b = 10^{-10}$ and $r = 0.08$, we have $\mathcal{R}_P = 0.1150 < 1$ and $\mathcal{R}_B = 8 > 1$. The time plots of the solutions are depicted in Figure 4. We can see that they converge to the positive equilibrium

$$\mathcal{E}_5 \approx (6.353 \times 10^7, \ 6206, \ 3984, \ 8.0 \times 10^4, \ 189.8, \ 0.0793, \ 1519, \ 768, 4.251 \times 10^6, \ 415.3, \ 1078, \ 16605, \ 1.055).$$

If we compare these simulations with the case when both $\mathcal{R}_P$ and $\mathcal{R}_B$ are less than one, we can see that there is a slight increment in all the pneumonia–susceptible compartments and a slight decrease in the pneumonia–infected compartments. The concentration of bacteria also reaches a lower value at the peak and at equilibrium.

Case 4. When $b = 9 \times 10^{-10}$ and $r = 0.08$, we have $\mathcal{R}_P = 1.0352 > 1$ and $\mathcal{R}_B = 8 > 1$. The time plots of the solutions are shown in Figure 5. We can see that the solutions converge to the positive equilibrium

$$\mathcal{E}_5 \approx (5.728 \times 10^7, \ 6007, \ 3867, \ 7.747 \times 10^4, \ 2186, \ 0.618, \ 1467, \ 744.4, 1.050 \times 10^7, \ 1102, \ 2074, \ 2.92 \times 10^4, \ 1.0497).$$

In this case, the number of hospitalised coinfected people becomes lower than in all other cases, while the non–hospitalised coinfected population reaches its highest value (although it still remains less than one individual at equilibrium). The concentration of bacteria in environment approaches a lower value at equilibrium in comparison to Cases 1–3.
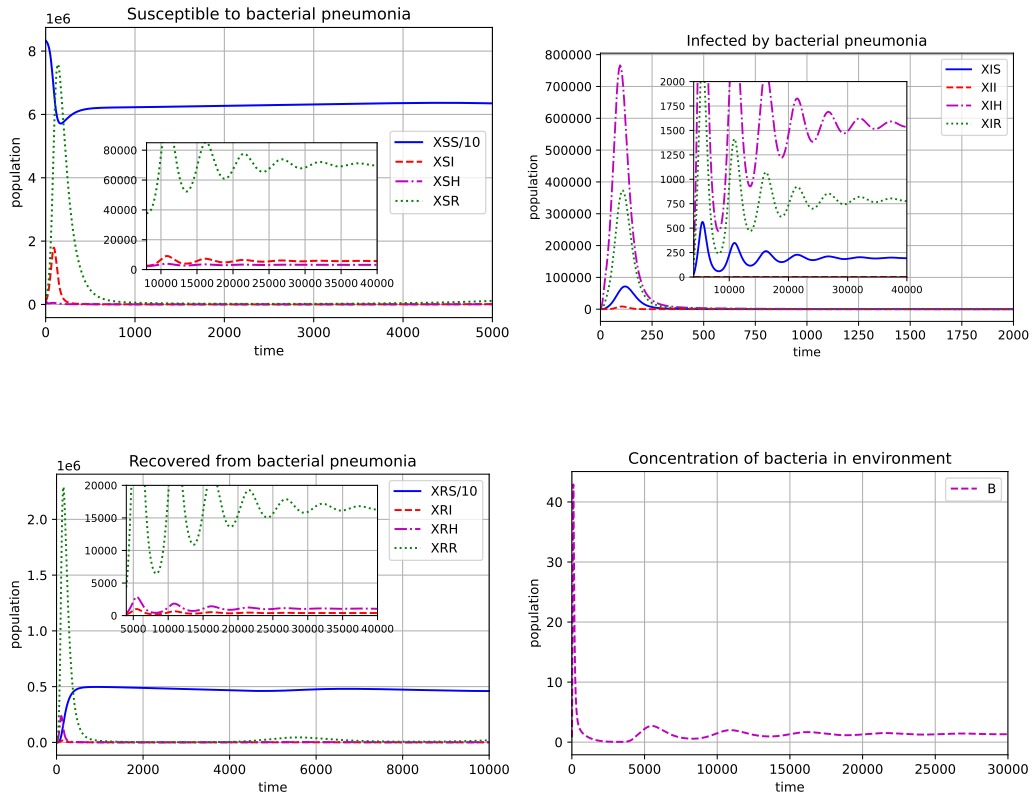
Figure 2. Dynamics of the coinfection model when $\mathcal{R}_C > 1$, $\mathcal{R}_P < 1$ and $\mathcal{R}_B < 1$.
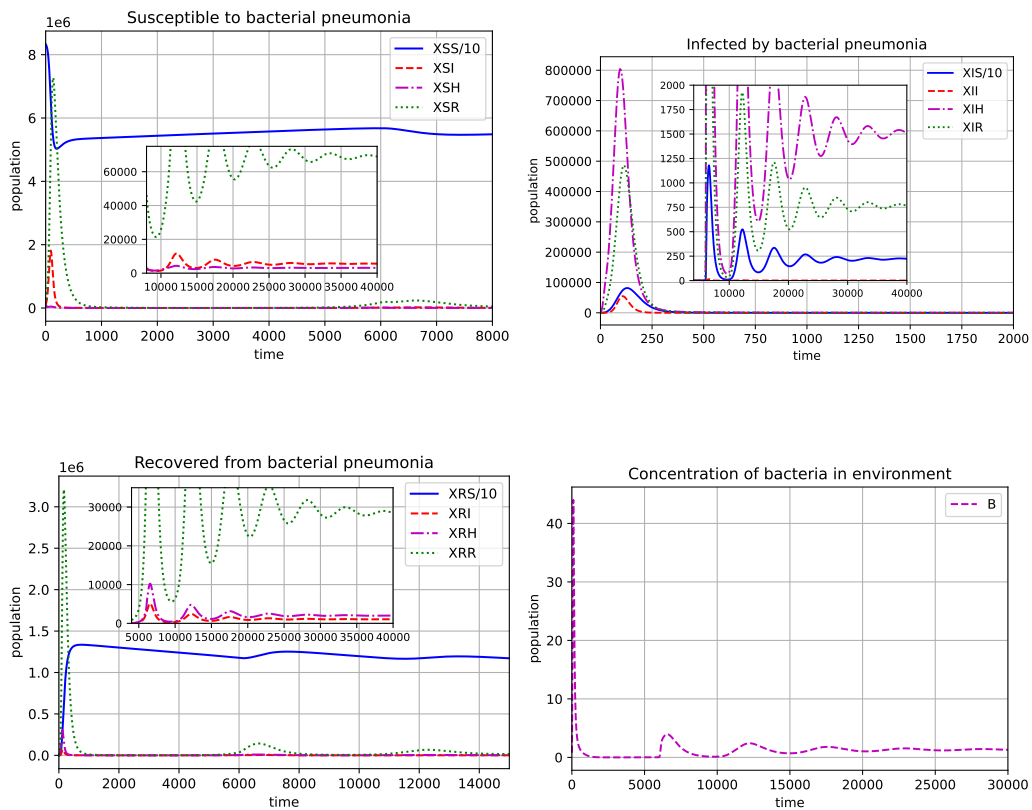

Figure 3. Dynamics of the coinfection model when $\mathcal{R}_C > 1$, $\mathcal{R}_P > 1$ and $\mathcal{R}_B < 1$.
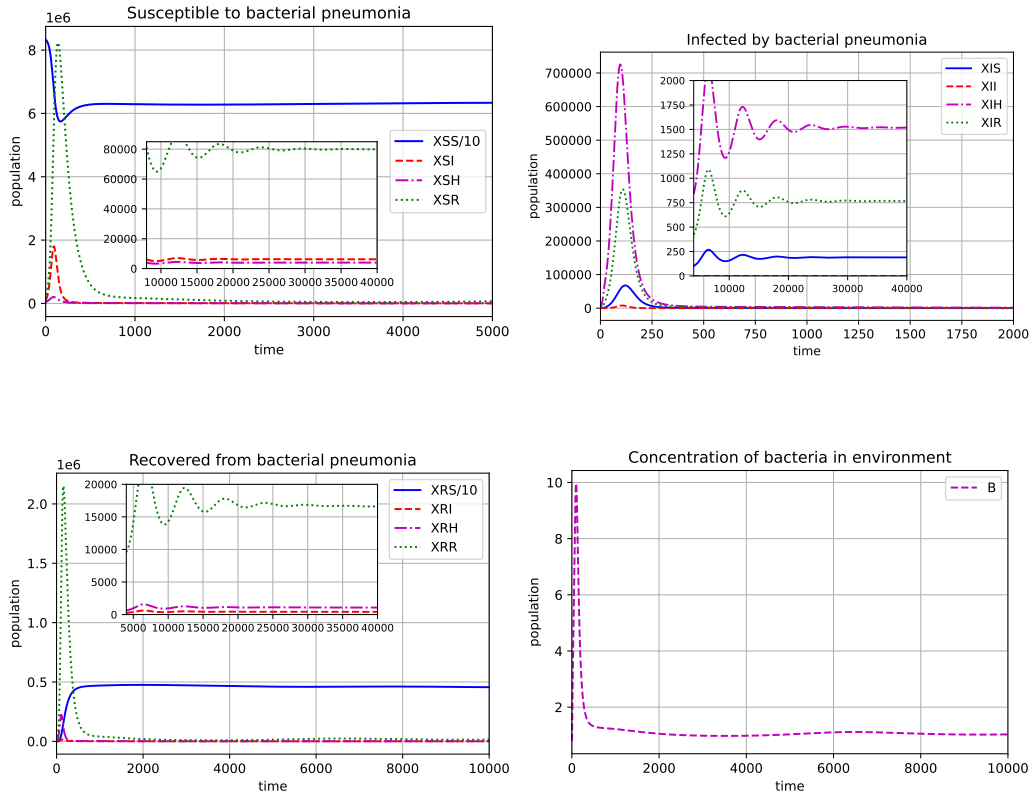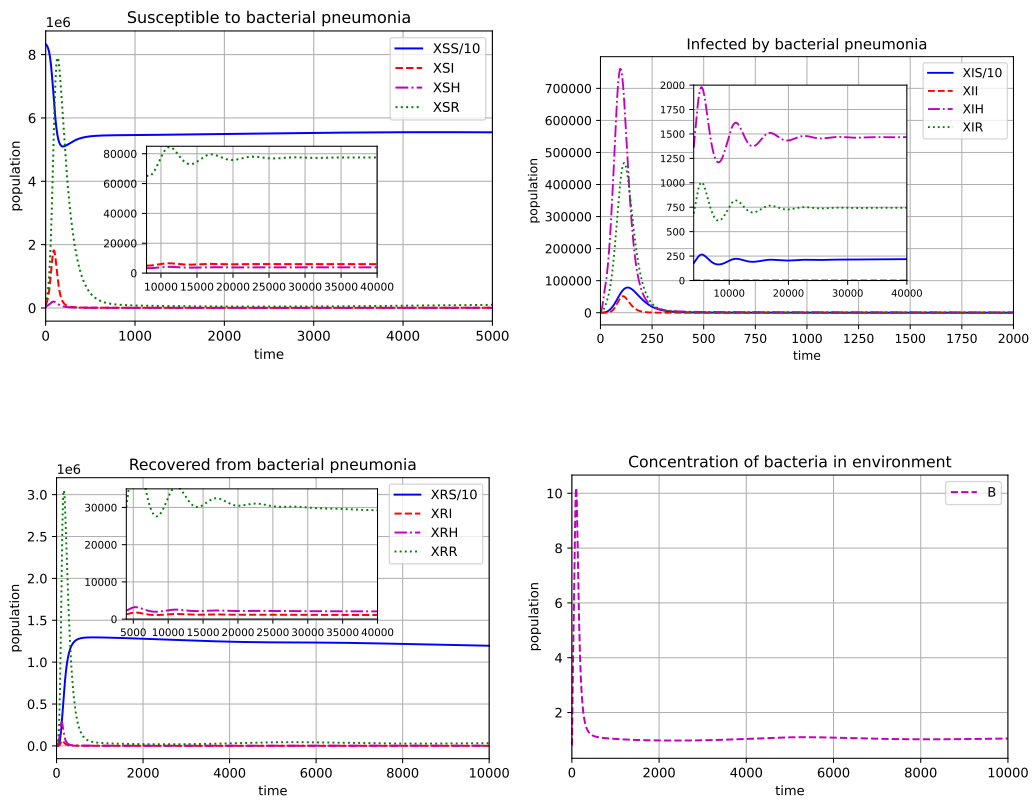
Figure 4. Dynamics of the coinfection model when $\mathcal{R}_C > 1$, $\mathcal{R}_P < 1$ and $\mathcal{R}_B > 1$.

Figure 5. Dynamics of the coinfection model when $\mathcal{R}_C > 1$, $\mathcal{R}_P > 1$ and $\mathcal{R}_B > 1$.

6 Results and discussion

In this work, we proposed a novel mathematical model to study the coinfection dynamics of COVID-19 and bacterial pneumonia. We established some basic properties of the sub-models (COVID-19 only and bacterial pneumonia only) and computed their basic reproduction numbers. We obtained some analytical results for the coinfection model and showed that its dynamics depend on three parameters: $\mathcal{R}_C$, $\mathcal{R}_P$ and $\mathcal{R}_B$.

We established in Theorem 4 that a necessary and sufficient condition to ensure that both diseases are eradicated from the population is to decrease $\mathcal{R}_C$ and $\mathcal{R}_P$ below unity. Biologically, this can be achieved by encouraging social distancing and wearing face masks. Moreover, part (ii) of Theorem 4 shows that a high reproduction number for the bacterial population in hospitals ($\mathcal{R}_B$) is not enough for bacterial pneumonia to persist in the population.

Furthermore, we determined the conditions for the existence of five equilibrium points. By means of numerical simulations, we showed that a sixth equilibrium may exist. Based on the simulations in Section 5, we conjecture that the COVID-19-present, pneumonia-present, bacterial population-present equilibrium $\mathcal{E}_5$ exists and is locally stable whenever $\mathcal{R}_C > 1$. This implies that both diseases can coexist in the population even if reproduction numbers of bacterial pneumonia ($\mathcal{R}_P$) and bacterial population ($\mathcal{R}_B$) are reduced below unity. Hence, epidemic policies should focus on reducing the basic reproduction number of COVID-19 in order to control the pandemic.

The simulations obtained in Section 5 show qualitatively similar dynamics for all four cases depicted in Figures 2–5: all subpopulations converge to a positive value. However, we must remark that the number of coinfected, non-hospitalised individuals (X_{II}) remains very low (less than one individual at equilibrium) in all cases; in contrast, most of the coinfection cases occur in the hospitalised compartment (X_{IH}). This is in line with the increased susceptibility of hospitalised COVID-19 patients to bacterial or fungal infections that has been observed in clinical trials [49, 50, 51].

Although many models have been proposed recently to study the coinfection dynamics of COVID-19 and other diseases [41, 42, 43, 44, 45, 46], our work is the first that takes into account the distinctive features of bacterial pneumonia, in particular, the inclusion of two infection ways (community and hospital transmission).

7 Conclusions

We proposed and analyzed an ODE model which, to the best of our knowledge, is the first epidemic model used to describe the coinfection of bacterial pneumonia and COVID-19. The highlights of our work include determining the stability conditions for the disease-free equilibria, as well as the existence conditions for five different equilibria. Due to the complexity of our model, we did not include a stability analysis for all equilibrium points. This is an area of research that could be elaborated on in future works. Other approaches that could be tackled in further research include expanding our coinfection model using vaccination against COVID-19 or multiple SARS-CoV-2 variants, as well as performing parameter fitting using real data.

Declarations

Code availability

The code used in this paper was written in Python and can be downloaded from `https://github.com/agcp26/COVID19-pneumonia`.

Consent for publication

Not applicable.

Conflicts of interest

The authors declare that they have no conflict of interests.

Funding

Not applicable.

Author's contributions

A.G.C.P.: Conceptualization, Methodology, Software, Formal Analysis, Writing - Original Draft, Writing - Review & Editing. D.A.O.: Conceptualization, Validation, Formal Analysis, Writing - Original Draft. All authors discussed the results and contributed to the final manuscript.

Acknowledgements

Not applicable.

References

[1] Nasir, N., Rehman, F., & Omair, S.F. Risk factors for bacterial infections in patients with moderate to severe COVID-19: A case-control study. *Journal of medical virology*, 93(7), 4564-4569, (2021). [CrossRef]

[2] Mirzaei, R., Goodarzi, P., Asadi, M., Soltani, A., Aljanabi, H.A.A., Jeda, A.S., ... & Karampoor, S. Bacterial co-infections with SARS-CoV-2. *IUBMB life*, 72(10), 2097-2111, (2020). [CrossRef]

[3] National Health Service, Respiratory tract infections (RTIs), https://www.nhs.uk/conditions/respiratory-tract-infection/ Access date: 19 November 2022.

[4] Hegazy, N.N., Mahrous, O.A., & Salah, M.A. An overview of respiratory tract infections in preschool children in primary healthcare. *Menoufia Medical Journal*, 31(3), 862, (2018). [CrossRef]

[5] Morens, D.M., Taubenberger, J.K., & Fauci, A.S. Predominant role of bacterial pneumonia as a cause of death in pandemic influenza: implications for pandemic influenza preparedness. *The Journal of infectious diseases*, 198(7), 962-970, (2008). [CrossRef]

[6] MacIntyre, C.R., Chughtai, A.A., Barnes, M., Ridda, I., Seale, H., Toms, R., & Heywood, A. The role of pneumonia and secondary bacterial infection in fatal and serious outcomes of pandemic influenza a (H1N1) pdm09. *BMC infectious diseases*, 18(1), 1-20, (2018). [CrossRef]

[7] Kumar, R., Bhattacharya, B., Meena, V., Soneja, M., & Wig, N. COVID-19 and TB co-infection-'Finishing touch''in perfect recipe to'severity'or 'death'. *Journal of Infection*, 81(3), e39-e40, (2020). [CrossRef]

[8] Lansbury, L., Lim, B., Baskaran, V., & Lim, W.S. Co-infections in people with COVID-19: a systematic review and meta-analysis. *Journal of Infection*, 81(2), 266-275, (2020). [CrossRef]

[9] Cox, M.J., Loman, N., Bogaert, D., & O'Grady, J. Co-infections: potentially lethal and unexplored in COVID-19. *The Lancet Microbe*, 1(1), e11, (2020). [CrossRef]

[10] Zhou, F., Yu, T., Du, R., Fan, G., Liu, Y., Liu, Z., ... & Cao, B. Clinical course and risk factors for mortality of adult inpatients with COVID-19 in Wuhan, China: a retrospective cohort study. *The lancet*, 395(10229), 1054-1062, (2020). [CrossRef]

[11] Chen, N., Zhou, M., Dong, X., Qu, J., Gong, F., Han, Y., ... & Zhang, L. Epidemiological and clinical characteristics of 99 cases of 2019 novel coronavirus pneumonia in Wuhan, China: a descriptive study. *The lancet*, 395(10223), 507-513, (2020). [CrossRef]

[12] Rawson, T.M., Moore, L.S., Zhu, N., Ranganathan, N., Skolimowska, K., Gilchrist, M., ... & Holmes, A. Bacterial and fungal coinfection in individuals with coronavirus: a rapid review to support COVID-19 antimicrobial prescribing. *Clinical infectious diseases*, 71(9), 2459-2468, (2020). [CrossRef]

[13] Bernoulli, D. Essai d'une nouvelle analyse de la mortalité causée par la petite vérole, et des avantages de l'inoculation pour la prévenir. *Histoire de l'Acad., Roy. Sci.(Paris) avec Mem*, 1-45, (1760).

[14] Ross, R. The prevention of malaria. *John Murray*, (1911).

[15] Ross, R. An application of the theory of probabilities to the study of a priori pathometry.—Part I. *Proceedings of the Royal Society of London. Series A, Containing papers of a mathematical and physical character*, 92(638), 204-230, (1916). [CrossRef]

[16] Ross, R., & Hudson, H.P. An application of the theory of probabilities to the study of a priori pathometry.–Part II. *Proceedings of the Royal Society of London. Series A, Containing papers of a mathematical and physical character*, 93(650), 212-225, (1917).

[17] Ross, R., & Hudson, H.P. An application of the theory of probabilities to the study of a priori pathometry.—Part III. *Proceedings of the Royal Society of London. Series A, Containing papers of a mathematical and physical character*, 93(650), 225-240, (1917). [CrossRef]

[18] Kermack, W.O., & McKendrick, A. G. A contribution to the mathematical theory of epidemics. Proceedings of the royal society of London. *Series A, Containing papers of a mathematical and physical character*, 115(772), 700-721, (1927). [CrossRef]

[19] House, T., & Keeling, M.J. Deterministic epidemic models with explicit household structure. *Mathematical biosciences*, 213(1), 29-39, (2008). [CrossRef]

[20] Becker, N. The uses of epidemic models. *Biometrics*, 35(1), 295-305, (1979). [CrossRef]

[21] Hethcote, H.W. The mathematics of infectious diseases. *SIAM review*, 42(4), 599-653, (2000). [CrossRef]

[22] Lee, G., Yoon, S.E., & Shin, K. Simple epidemic models with segmentation can Be better than complex ones. *Plos one*, 17(1), e0262244, (2022). [CrossRef]

[23] Allegretti, S., Bulai, I.M., Marino, R., Menandro, M.A., & Parisi, K. Vaccination effect conjoint to fraction of avoided contacts for a Sars-Cov-2 mathematical model. *Mathematical Modelling and Numerical Simulation with Applications*, 1(2), 56-66, (2021). [CrossRef]

[24] Ikram, R., Khan, A., Zahri, M., Saeed, A., Yavuz, M., & Kumam, P. Extinction and stationary distribution of a stochastic COVID-19 epidemic model with time-delay. *Computers in Biology and Medicine*, 141, 105115, (2022). [CrossRef]

[25] Sinan, M., Leng, J., Anjum, M., & Fiaz, M. Asymptotic behavior and semi-analytic solution of a novel compartmental biological model. *Mathematical Modelling and Numerical Simulation with Applications*, 2(2), 88-107, (2022). [CrossRef]

[26] Yavuz, M., Coşar, F.Ö., Günay, F., & Özdemir, F.N. A new mathematical modeling of the COVID-19 pandemic including the vaccination campaign. *Open Journal of Modelling and Simulation*, 9(3), 299-321, (2021). [CrossRef]

[27] Özköse, F., & Yavuz, M. Investigation of interactions between COVID-19 and diabetes with hereditary traits using real data: A case study in Turkey. *Computers in biology and medicine*, 141, 105044, (2022). [CrossRef]

[28] Özköse, F., Yavuz, M., Şenel, M.T., & Habbireeh, R. Fractional order modelling of omicron SARS-CoV-2 variant containing heart attack effect using real data from the United Kingdom. *Chaos, Solitons & Fractals*, 157, 111954, (2022). [CrossRef]

[29] Orozco, J.A.M., Tinajero, Á.S., Vargas, E.B., Cueva, A.I.D., Escobar, H.R., Alcocer, E.V., ... & Santillán, D.P.R. COVID-19 and tuberculosis coinfection in a 51-year-old taxi driver in Mexico city. *The American journal of case reports*, 21, e927628-1, (2020). [CrossRef]

[30] Tadolini, M., Codecasa, L.R., García-García, J.M., Blanc, F.X., Borisov, S., Alffenaar, J.W., ... & Migliori, G.B. Active tuberculosis, sequelae and COVID-19 co-infection: first cohort of 49 cases. *European Respiratory Journal*, 56(1), (2020). [CrossRef]

[31] Yadav, S., & Rawal, G. The case of pulmonary tuberculosis with COVID-19 in an Indian male-a first of its type case ever reported from South Asia. *Pan African Medical Journal*, 36(1), (2020). [CrossRef]

[32] Khurana, A.K., & Aggarwal, D. The (in) significance of TB and COVID-19 co-infection. *European Respiratory Journal*, 56(2), (2020). [CrossRef]

[33] Petrone, L., Petruccioli, E., Vanini, V., Cuzzi, G., Gualano, G., Vittozzi, P., ... & Goletti, D. Coinfection of tuberculosis and COVID-19 limits the ability to in vitro respond to SARS-CoV-2. *International Journal of Infectious Diseases*, 113, S82-S87, (2021). [CrossRef]

[34] Lew, S., Manes, P., & Smith, B. Coinfection with SARS-CoV-2 and influenza A virus in a 32-year-old man. *The American Journal of Case Reports*, 21, e926092-1, (2020). [CrossRef]

[35] Jing, R., Vunnam, R.R., Schnaubelt, E., Vokoun, C., Cushman-Vokoun, A., Goldner, D., & Vunnam, S.R. Co-infection of COVID-19 and influenza A in a hemodialysis patient: a case report. *BMC Infectious Diseases*, 21(1), 1-6, (2021). [CrossRef]

[36] Fahim, M., Ghonim, H.A.E.S., Roshdy, W.H., Naguib, A., Elguindy, N., AbdelFatah, M., ... & Eid, A. Coinfection with SARS-CoV-2 and influenza A (H1N1) in a patient seen at an influenza-like illness surveillance site in Egypt: case report. *JMIR public health and surveillance*, 7(4), e27433, (2021). [CrossRef]

[37] Xiang, X., Wang, Z.H., Ye, L.L., He, X.L., Wei, X.S., Ma, Y.L., ... & Zhou, Q. Co-infection of SARS-COV-2 and influenza A virus: a case series and fast review. *Current Medical Science*, 41(1), 51-57, (2021). [CrossRef]

[38] Ata, F., Yousaf, Q., Parambil, J.V., Parengal, J., Mohamedali, M.G., & Yousaf, Z. A 28-year-old man from India with SARS-Cov-2 and pulmonary tuberculosis co-infection with central nervous system involvement. *The American journal of case reports*, 21, e926034-1, (2020). [CrossRef]

[39] Elhazmi, A., Al-Tawfiq, J.A., Sallam, H., Al-Omari, A., Alhumaid, S., Mady, A., & Al Mutair, A. Severe acute respiratory syndrome coronavirus 2 (SARS-CoV-2) and Middle East Respiratory Syndrome Coronavirus (MERS-CoV) coinfection: A unique case series. *Travel Medicine and Infectious Disease*, 41, 102026, (2021). [CrossRef]

[40] Giannella, M., Rinaldi, M., Tesini, G., Gallo, M., Cipriani, V., Vatamanu, O., ... & Curti, S. Predictive model for bacterial co-infection in patients hospitalized for COVID-19: A multicenter observational cohort study. *Infection*, 50, 1243–1253, (2022). [CrossRef]

[41] Soni, B., & Singh, S. COVID-19 co-infection mathematical model as guided through signaling structural framework. *Computational and Structural Biotechnology Journal*, 19, 1672-1683, (2021). [CrossRef]

[42] Tchoumi, S.Y., Diagne, M.L., Rwezaura, H., & Tchuenche, J.M. Malaria and COVID-19 co-dynamics: A mathematical model and optimal control. *Applied mathematical modelling*, 99, 294-327, (2021). [CrossRef]

[43] Bandekar, S.R., & Ghosh, M. A co-infection model on TB-COVID-19 with optimal control and sensitivity analysis. *Mathematics and Computers in Simulation*, 200, 1-31, (2022). [CrossRef]

[44] Rwezaura, H., Diagne, M.L., Omame, A., de Espindola, A.L., & Tchuenche, J.M. Mathematical modeling and optimal control of SARS-CoV-2 and tuberculosis co-infection: a case study of Indonesia. *Modeling Earth Systems and Environment*, 8(4), 5493-5520, (2022). [CrossRef]

[45] Omame, A., Rwezaura, H., Diagne, M.L., Inyama, S.C., & Tchuenche, J.M. COVID-19 and dengue co-infection in Brazil: optimal control and cost-effectiveness analysis. *The European Physical Journal Plus*, 136(10), 1-33, (2021). [CrossRef]

[46] Omame, A., Nwajeri, U.K., Abbas, M., & Onyenegecha, C.P. A fractional order control model for Diabetes and COVID-19 co-dynamics with Mittag-Leffler function. *Alexandria Engineering Journal*, 61(10), 7619-7635, (2022). [CrossRef]

[47] Sampson, S. and De Pietro, M. What to know about bacterial pneumonia, https://www.medicalnewstoday.com/articles/312565, Access date: 31 August 2022.

[48] Sethi, S. Hospital-acquired pneumonia, https://www.msdmanuals.com/home/lung-and-airway-disorders/pneumonia/hospital-acquired-pneumonia, Access date: 31 August 2022.

[49] Ansari, S., Hays, J.P., Kemp, A., Okechukwu, R., Murugaiyan, J., Ekwanzala, M.D., ... & van Dongen, M.B. The potential impact of the COVID-19 pandemic on global antimicrobial and biocide resistance: an AMR Insights global perspective. *JAC-Antimicrobial Resistance*, 3(2), dlab038, (2021). [CrossRef]

[50] Huang, C., Wang, Y., Li, X., Ren, L., Zhao, J., Hu, Y., ... & Cao, B. Clinical features of patients infected with 2019 novel coronavirus in Wuhan, China. *The lancet*, 395(10223), 497-506, (2020). [CrossRef]

[51] Wang, D., Hu, B., Hu, C., Zhu, F., Liu, X., Zhang, J., ... & Peng, Z. Clinical characteristics of 138 hospitalized patients with 2019 novel coronavirus–infected pneumonia in Wuhan, China. *Jama*, 323(11), 1061-1069, (2020). [CrossRef]

[52] Van den Driessche, P., & Watmough, J. Reproduction numbers and sub-threshold endemic equilibria for compartmental models of disease transmission. *Mathematical biosciences*, 180(1-2), 29-48, (2002). [CrossRef]

[53] Chicone, C. *Types of Differential Equations. Ordinary Differential Equations with Applications* (Vol. 34). Springer: New York, (1999).

[54] Oluyori, D.A., Adebayo, H.O., & Pérez, Á.G. Global analysis of an SEIRS model for COVID-19 capturing saturated incidence with treatment response. *Applications and Applied Mathematics: An International Journal (AAM)*, 16(2), 9, (2021). [CrossRef]

Mathematical Modelling and Numerical Simulation with Applications (MMNSA) (https://www.mmnsa.org)